ACS OMEGA

http://pubs.acs.org/journal/acsodf

Article

Hydroxyethyl Chitosan-Reinforced Polyvinyl Alcohol/Biphasic Calcium Phosphate Hydrogels for Bone Regeneration

Lei Nie,*,¶ Yaling Deng,¶ Pei Li, Ruixia Hou, Amin Shavandi,* and Shoufeng Yang

Cite This: *ACS Omega* 2020, 5, 10948−10957

Read Online

ACCESS | Metrics & More | Article Recommendations | Supporting Information

ABSTRACT: Fabrication of reinforced scaffolds for bone regeneration remains a significant challenge. The weak mechanical properties of the chitosan (CS)-based composite scaffold hindered its further application in clinic. Here, to obtain hydroxyethyl CS (HECS), some hydrogen bonds of CS were replaced by hydroxyethyl groups. Then, HECS-reinforced polyvinyl alcohol (PVA)/biphasic calcium phosphate (BCP) nanoparticle hydrogel was fabricated via cycled freeze-thawing followed by an *in vitro* biomineralization treatment using a cell culture medium. The synthesized hydrogel had an interconnected porous structure with a uniform pore distribution. Compared to the CS/PVA/BCP hydrogel, the HECS/PVA/BCP hydrogels showed a thicker pore wall and had a compressive strength of up to 5−7 MPa. The biomineralized hydrogel possessed a better compressive strength and cytocompatibility compared to the untreated hydrogel, confirmed by CCK-8 analysis and fluorescence images. The modification of CS with hydroxyethyl groups and *in vitro* biomineralization were sufficient to improve the mechanical properties of the scaffold, and the HECS-reinforced PVA/BCP hydrogel was promising for bone tissue engineering applications.

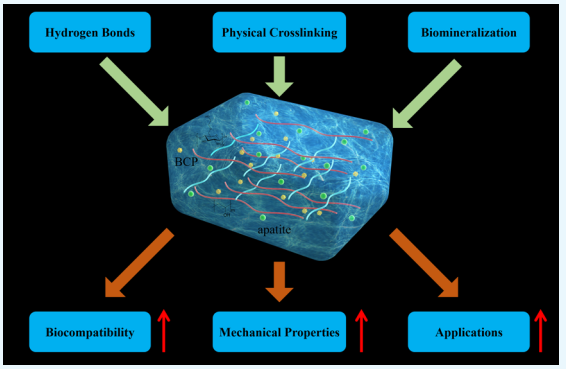

1. INTRODUCTION

Natural bone has an excellent self-regeneration ability with desired mechanical properties. However, critical-sized bone defects may arise from congenital and acquired pathologies such as trauma, tumor, infection, or bone-related disease that cannot heal through normal physiological processes, and surgical intervention is required to achieve healing.[1,2] Autografts as one current treatment option are restricted by the graft size and have the risk of donor site morbidities such as infection and ongoing pain following the surgery.[3] Allografts as another treatment option have the potential risk of disease transmission and immune response.[4] To eliminate the limitations of the current therapies, bone tissue engineering (BTE) offers promising alternatives. With this regard, the three-dimensional (3D) porous scaffold with appropriate physical, mechanical, and biological properties has been utilized to aid and promote bone regeneration.[5−8] The mechanical properties such as compressive strength are vital for cellular interactions, as the scaffold needs to tolerate internal stress until bone tissue regeneration takes place.[9]

Various materials, including metals, ceramics, polymers, and their composites, have been utilized in the fabrication of bone scaffolds.[5] Calcium phosphate (CaP) bioceramics have been widely used because of the excellent bioactivity, osteoconductivity, and compositional similarities to bone mineral.[10,11] Calcium phosphate (CaP) is resorbed in vivo and releases calcium and phosphate ions. These ions can regulate bone formation through osteoinduction.[12,13] Synthetic calcium phosphate-based ceramics mainly include biphasic calcium phosphate (BCP),[14,15] hydroxyapatite (HA),[16] and β-tricalcium phosphate (β-TCP).[17−20] BCP, as a mixture of HA and β-TCP, is considered a suitable material for making bone scaffolds because of its controllable degradation, allowing bone regeneration and growth.[14,17,21,22] However, the inherent brittleness of the BCP-based scaffold limits its utilization, especially for load-bearing applications.[23,24]

The mechanical strength of BCP-based scaffolds can be improved via introducing polymeric materials[25−29] such as polyvinyl alcohol (PVA), which is widely used in biomedical applications and offers a high degree of swelling in aqueous solvents.[30] The abundance of hydroxyl groups attached to the PVA carbon chain backbone supports its hydrogen bonding with bioceramic nanoparticles (NPs).

In our previous research, the surface hydroxyl groups on BCP NPs energetically interacted with PVA macromolecules, forming the interfacial layer, and we could develop BCP/PVA scaffolds with tunable compressive strength and porosity via changing the weight ratio of BCP/PVA.[31] In another study,

Received: February 19, 2020
Accepted: April 24, 2020
Published: May 6, 2020

BCP/PVA scaffolds were fabricated by fused deposition modeling, which showed excellent mechanical properties, reported to be due to improved interfacial interactions of PVA and BCP.[32]

Based on the interaction of PVA and BCP NPs, the second polymer chain can be introduced to further improve the scaffold mechanical properties.[33,34] Chitosan (CS) is a versatile polymer formed by glucosamine and *N*-acetyl glucosamine linked with a β-1-4-glycosidic linkage. CS has been especially attractive to BTE because it supports the attachments and proliferation of osteoblast cells as well as the formation of a mineralized bone matrix *in vitro*.[35−37] Besides, it is biocompatible and biodegradable in the human body with nontoxic degradation products.[38,39] A pure CS scaffold has low mechanical properties limiting its potential clinical applications. However, hydrogen bond formation between the hydroxyl group of PVA and the primary amine group of CS resulted in the PVA/CS hydrogels with a higher mechanical strength compared to the pure CS.[40,41]

In addition, the highly polar hydroxyl groups in the chemical structure of PVA and CS tend to form inter- and intramolecular hydrogen bonds that promote the localized stability and miscibility of CS and PVA.[42,43] Our previous study showed that the CS/gelatin/BCP hydrogel had an excellent compressive strength (1.2−2.5 MPa), which was because of uniform dispersion of BCP NPs into the composites and physical cross-linking with CS and gelatin.[27] However, the poor solubility of CS in physiological solvents has dramatically limited its biomedical application as the protonation of primary amino groups happens in an acidic solution, further hindering the improvement of its mechanical properties.[44] Therefore, it is necessary to make CS water-soluble to improve its mechanical properties.

In this study, part of hydrogen bonds in CS was replaced with hydroxyethyl groups to obtain water-soluble HECS. The HECS/PVA/BCP hydrogel was then fabricated via cycled freeze-thawing, and later, the reinforced hydrogel was acquired by *in vitro* biomineralization treatment through immersing it in a cell culture medium (Scheme 1). The physicochemical characteristics and biological properties of hydrogels were systematically investigated. Besides, the reinforcing mechanism of HECS/PVA/BCP hydrogels was studied.

Scheme 1. Schematic Illustration of the Fabrication and Biomineralization Process of the HECS/PVA/BCP Scaffold

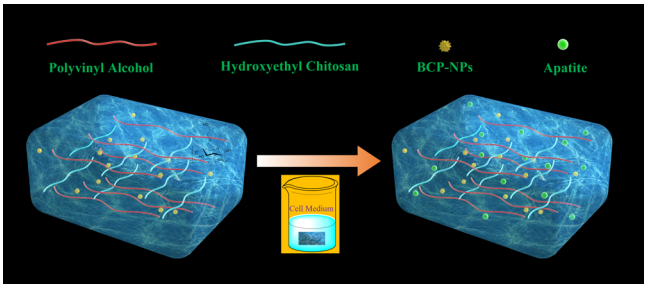

2. RESULTS AND DISCUSSION

2.1. FTIR Analysis of HECS and BCP NPs. The Fourier transform infrared (FTIR) spectroscopy spectra of CS and HECS are shown in Figure 1A. For pure CS, the characteristic peak at 3355 cm^{-1} was attributed to the stretching vibration of $-NH_2$ and $-OH$ groups in CS. The bands at 2875 and 1655 cm^{-1} were assigned to the stretching vibration of C−H and bending vibration of N−H, respectively. The peaks located at 1149 and 1069 cm^{-1} were ascribed to the bridge-O stretching vibration and C−O stretching vibration.[45] In the spectrum of HECS, the obvious $-CH_2-$ bending vibration was detected at 1456 cm^{-1}. The intensification and shift of −OH stretching vibration at 3377 cm^{-1}, stretching vibration of C−H at 2888 cm^{-1}, and C−O stretching vibration at 1086 cm^{-1} confirmed the existence of the hydroxyethyl group.[46,47] The FTIR results with the addition of ^{1}H NMR analysis for HECS (Supporting Information, Figure S2) demonstrated the successful hydroxyethylation of CS. The FTIR spectra of PVA, HECS, BCP, and hydrogels with different compositions are exhibited in Figure 1B. The spectrum of PVA shows its characteristic absorption peaks at 3286 cm^{-1} (O−H stretching vibration), 2910 cm^{-1} (C−H stretching vibration), 1419 cm^{-1} (C−C stretching vibration), 1085 cm^{-1} (C−O stretching vibration), and 838 cm^{-1} (C−H rocking vibration). For the FTIR spectrum of BCP, the peaks of phosphate ions as the principal molecular components in HA and β-TCP (PO_4^{3-}) appeared in the 1200−550 cm^{-1} regions. All characteristic peaks of PVA (3286, 2910, 1419, and 1085 cm^{-1}), HECS (3377, 2888, 1643, and 1086 cm^{-1}), and BCP (1070^{-} and 727 cm^{-1}) were observed in the hydrogels (Figure 1C). Besides, a slight shift in the characteristic peaks (3347, 2939, 1646, 1423, and 1079 cm^{-1}) for all the samples occurred because of the strong interaction between surface OH groups. The N−H and C−H stretch at 2362 cm^{-1} in the FTIR spectrum of hydrogels confirms the formation of hydrogen bonds between HECS, PVA, and BCP NPs.[48]

2.2. Characterization of BCP NPs. The morphological and crystalline properties of BCP NPs were investigated by transmission electron microscopy (TEM) (Figure 2A,B) and X-ray diffraction (XRD) (Supporting Information, Figure S3) analysis. TEM images showed the irregular form of BCP NPs, which was different from our previous published studies (needle-like morphology of BCP NPs).[27] Compared to the needle-shaped NPs, the random-shaped NPs own a higher specific surface area and further improve the interaction with HECS and PVA. Also, the XRD analysis confirmed that the HA/β-TCP ratio was about 40:60.

2.3. Morphology and Microstructure Analysis of the HECS/PVA/BCP Hydrogel. Porous hydrogels have an important role in the construction of bone engineering and new bone regeneration during *in vivo* processes. The porous structure provides the template for cell attachment and bone extracellular matrix formation. The porous network structure of the prepared HECS/PVA/BCP hydrogel was observed via scanning electron microscopy (SEM) images, as shown in Figure 3. Compared to CS/PVA/BCP hydrogels (Supporting Information, Figure S4), the HECS/PVA/BCP hydrogels showed regular and tight pores, and the range of pore diameter was 0.4−82.6 μm, which was calculated using ImageJ software (Supporting Information, Figures S5 and S6). Besides, the irregular porous structure with microsize pores was observed on the pore walls. With the decrease in HECS concentration (from 18.18 to 8.70%), a more uniform pore distribution was formed.

2.4. Porosity and Compressive Strength Analysis of the HECS/PVA/BCP Hydrogel. The porosity of the scaffold was considered as the main parameter for bone replacement. The porosity of all prepared HECS/PVA/BCP scaffolds was

https://dx.doi.org/10.1021/acsomega.0c00727
ACS Omega 2020, 5, 10948−10957

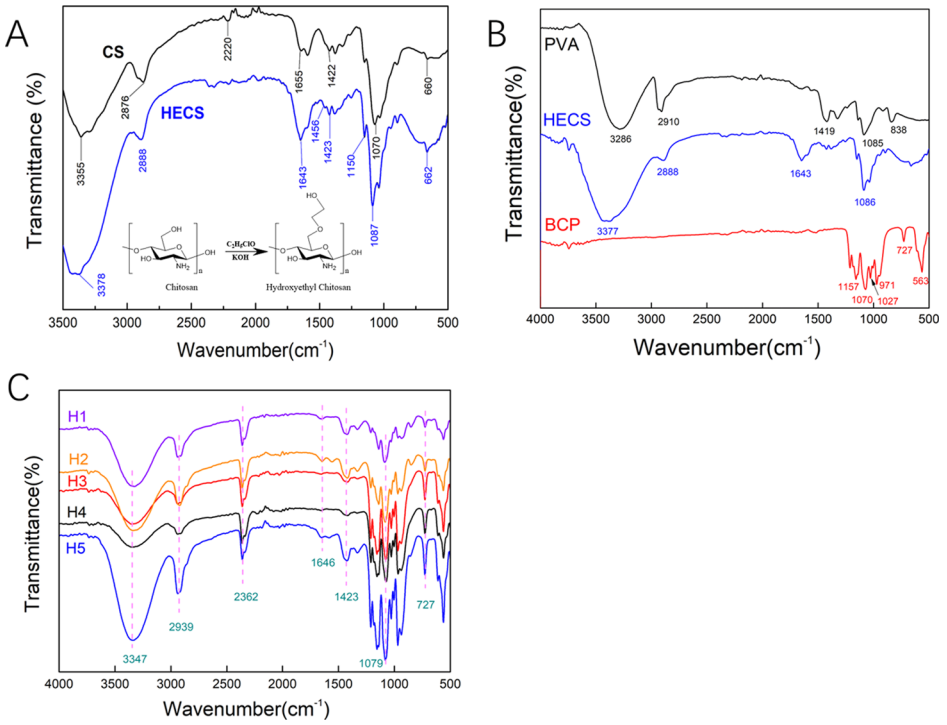

Figure 1. (A) FTIR spectra of CS and HECS; (B) FTIR spectra of pure PVA, HECS, and BCP NPs; and (C) FTIR spectra of the prepared HECS/PVA/BCP hydrogels; H1, H2, H3, H4, and H5 represent the different hydrogels prepared using different HECS/PVA/BCP ratios.

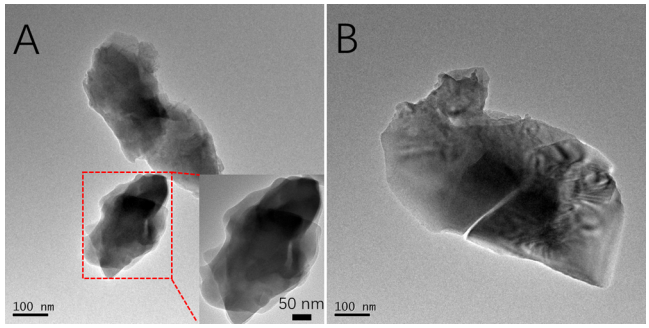

Figure 2. TEM images of BCP NPs (A,B), the inset at the right bottom of (A) was enlarged at a higher magnification.

higher than 40%, and with the decrease in HECS concentration, the porosity of the scaffold increased from 45.36 to 49.68%, as shown in Figure 4A. The sample H3 displayed the highest porosity (60.59%) at the HECS concentration of 13.33%. It is difficult to find a trade-off on porosity and mechanical property for a porous scaffold, and the compressive strength of the scaffold usually decreases with increasing its porosity.[49] The compressive strength (Figure 4B) of all prepared HECS/PVA/BCP scaffolds in this study was in the range of 5−7 MPa, which was higher than the compressive strength of CS/PVA/BCP (about 2.5−3.0 MPa, Supporting Information, Figure S7). Moreover, the compressive strength of about 2.22 MPa was previously reported for CS/PVA/β-TCP.[50] The obtained compressive strength in this study (5−7 MPa) was higher than the BCP NP-based scaffold in our previous papers (0.2−0.4 MPa) as well. This higher mechanical property is due to the introduction of HECS and the irregular shape of BCP NPs that are used in this study.[27,51] The sample H4 exhibited the highest compressive strength of 6.85 ± 1.06 MPa, and the sample H5 with the lowest concentration (8.70%) of HECS displayed the lowest compressive strength of 5.58 ± 0.44 MPa. The compressive strength initially increased and then decreased, with the decreasing concentration of HECS. The obtained scaffold did not show the typical reciprocal relationship between porosity and compressive strength, mainly attributed to the regular and tight porous structure.

2.5. Swelling Properties of the HECS/PVA/BCP Hydrogel. The swelling behavior of the HECS/PVA/BCP hydrogel in phosphate-buffered saline (PBS) was recorded and is shown in Figure 5. The swelling ratio of all hydrogels increased very fast at the beginning of 20 min and then began to stabilize and reached an equilibrium state at 120 min. There was no significant difference in hydrogels with different compositions; the equilibrium swelling ratio for all samples was in the range of 82−89%. Compared to the equilibrium swelling ratio of CS/PVA/BCP hydrogels (80−90%), the HECS/PVA/BCP hydrogels did not show noticeable change.

2.6. Morphology Analysis of the Biomineralized HECS/PVA/BCP Hydrogel. After *in vitro* biomineralization treatment, the HECS/PVA/BCP hydrogels maintained their interconnected porous structure; however, the morphology of the pore wall changed compared to that of untreated samples. Dulbecco's modified Eagle's medium (DMEM) with fetal bovine serum (FBS) was proved to be effective for biomineralization and the formation of bone-like apatite.[52] After immersing the hydrogels in the cell medium for 5 days, apatite crystals on the surface of hydrogels were observed (Figure 6), as well as some apparent aggregations of apatite species, compared to untreated hydrogels (Figure 3). The apatite formed on the surface was compact, which could further reinforce the hydrogels. The apatite particle sizes observed were around 1−2 μm in diameter. The hydrogel at the lowest concentration of HECS (8.70%) presented a smoother surface compared to other samples.

https://dx.doi.org/10.1021/acsomega.0c00727
ACS Omega 2020, 5, 10948−10957

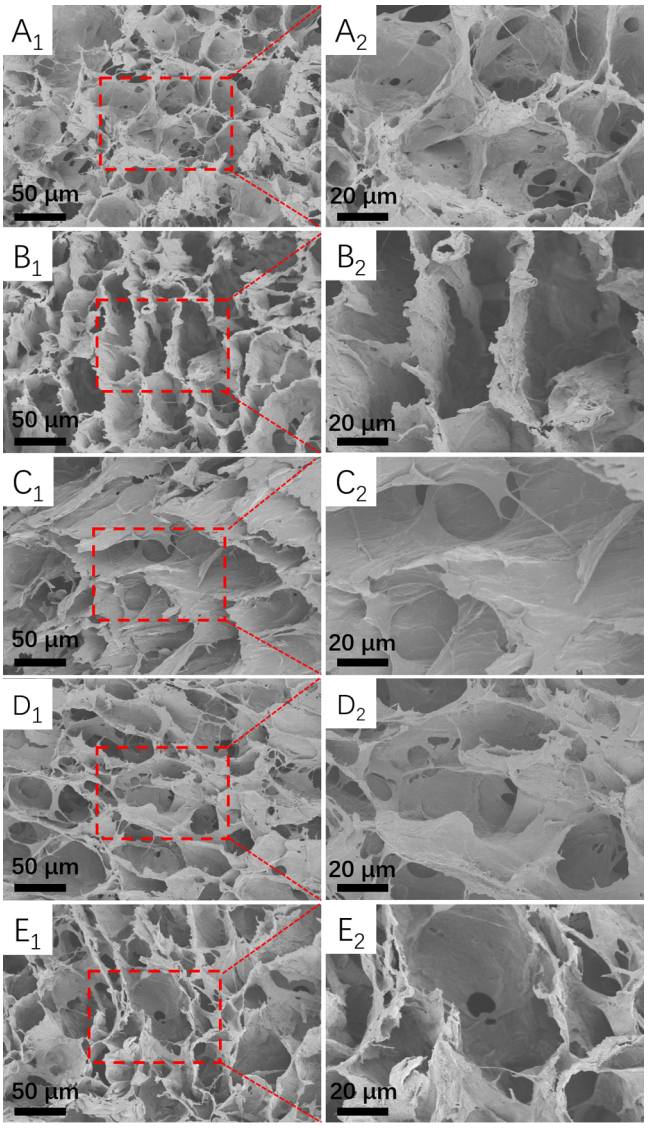

Figure 3. SEM images of the prepared HECS/PVA/BCP hydrogels, the cross-sectional morphology was observed for all samples: (A_1,A_2) hydrogel H1; (B_1,B_2) hydrogel H2; (C_1,C_2) hydrogel H3; (D_1,D_2) hydrogel H4; and (E_1,E_2) hydrogel H5.

2.7. Porosity and Compressive Strength of the Biomineralized HECS/PVA/BCP Hydrogel. After *in vitro* biomineralization treatment, the porosity of HECS/PVA/BCP hydrogels was investigated (Figure 7A). Except for sample

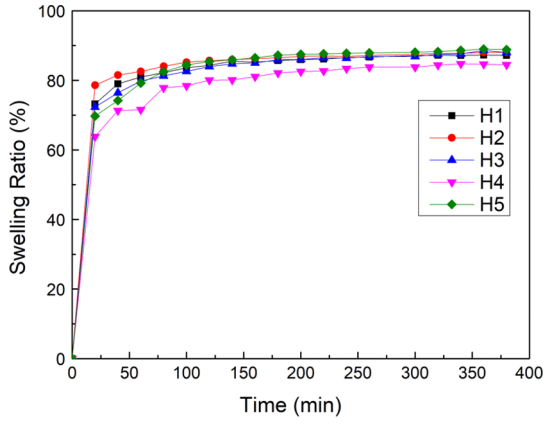

Figure 5. Swelling behavior of HECS/PVA/BCP scaffolds after soaking in PBS.

$_B$H4, the porosity of the hydrogel was lower than that of the unbiomineralized ones (48.67%). The porosity of $_B$H4 was about 56.28%, and the porosity of H4 was around 50%. Besides, hydrogel $_B$H1 with the HECS concentration of 18.18% had the lowest porosity of 35.53%. The compressive strength of the hydrogel after biomineralization was measured (Figure 7B). Compared to our previous research, the different testing method was used because of the fracture point appeared during the compression process.[27,28] Compared with the unmineralized hydrogel (Figure 4B), the compressive strength of hydrogels was 2−3 MPa higher and the value was improved to 7−8 MPa. The sample $_B$H5 with the HECS concentration of 8.7% had the highest value, 7.95 MPa. At the 13.33% of HECS, the hydrogel $_B$H3 showed the lowest compressive strength of about 7.17 MPa.

2.8. Cytotoxicity Evaluation. The CCK-8 assay was used to evaluate the cell toxicity of the hydrogel. In our research, hBMSCs were cultured with biomineralized hydrogels for 1, 3, and 5 days (Figure 8). It showed that the absorbance value at 570 nm of all hydrogels increased with increasing culturing days, indicating that cells grew and proliferated on the hydrogel. Compared to CS/PVA/BCP hydrogels and HECS/PVA/BCP hydrogels without biomineralization treatment (Supporting Information, Figures S8 and S9), the cultured hBMSCs had faster growth in biomineralized HECS/PVA/BCP hydrogels compared to unbiomineralized hydrogels. At day 5, the morphology of cells in the hydrogels was assessed using the fluorescent staining [phalloidin-FITC/4,6-diamidino-2-phenylindole (DAPI)] (Figure 9). DAPI stained the nucleus of the cultured cells in blue, and the

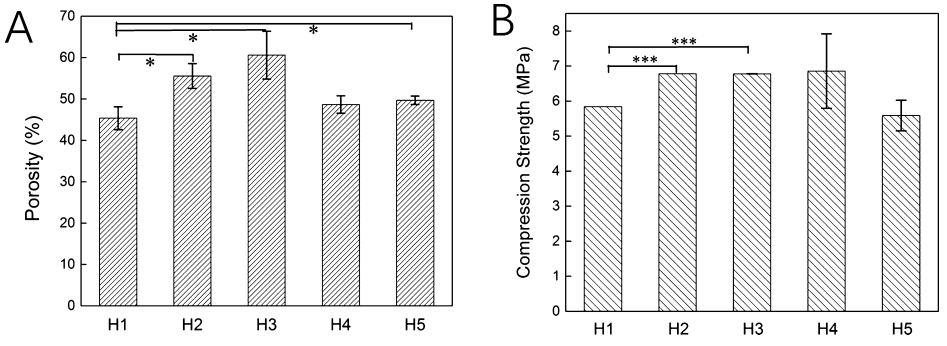

Figure 4. Porosity (A) and compressive strength (B) of the HECS/PVA/BCP scaffolds.

https://dx.doi.org/10.1021/acsomega.0c00727
ACS Omega 2020, 5, 10948−10957

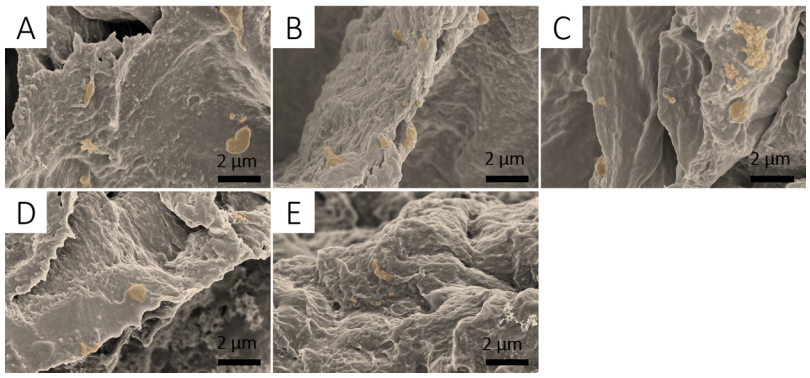

Figure 6. SEM images of the prepared HECS/PVA/BCP hydrogels after *in vitro* biomineralization treatment using cell medium: (A): $_{B}$H1; (B): $_{B}$H2; (C) $_{B}$H3; (D) $_{B}$H4; and (E) $_{B}$H5. The aggregations of apatite crystals were marked in a different color.

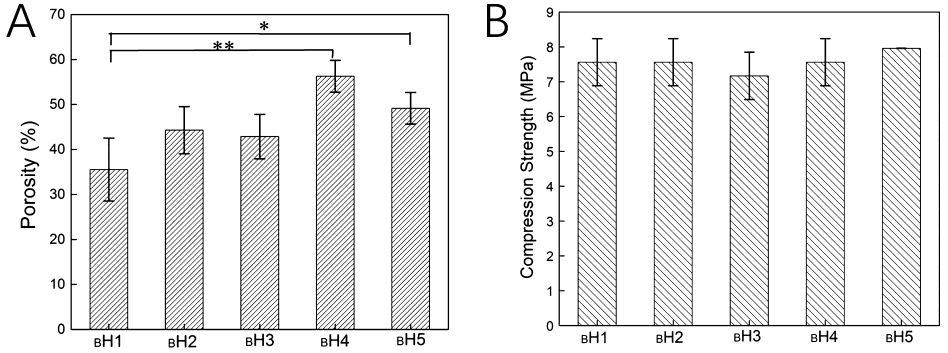

Figure 7. (A) Porosity and (B) compressive strength of the prepared HECS/PVA/BCP hydrogels after *in vitro* biomineralization treatment.

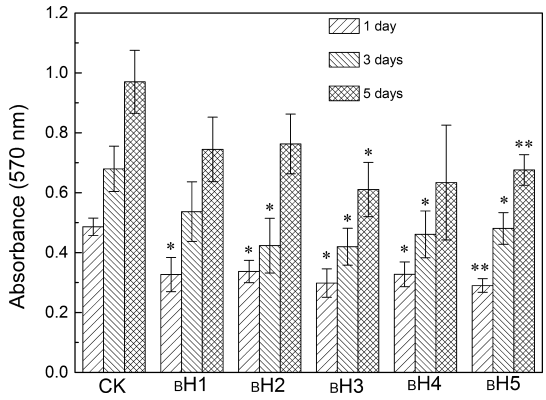

Figure 8. In vitro cytocompatibility of the prepared HECS/PVA/BCP hydrogels after *in vitro* biomineralization via culturing with human bone marrow-derived mesenchymal stem cells (hBMSCs) for different days, OD_{570nm} values were recorded after being treated using CCK-8 kit solutions, and the cells without hydrogels were considered as a control check group (CK).

cytoplasm was stained by phalloidin-FITC in green. hBMSCs had grown inside the hydrogels, and a certain number of cells were watched for all hydrogels. Given the presence of polysaccharide (HECS) in the hydrogels, the framework of the prepared HECS/PVA/BCP hydrogels was stained in green as well. From the fluorescent staining result, the HECS/PVA/BCP hydrogels displayed an interconnected porous structure.

2.9. Reinforced Mechanism. The hydroxyethyl groups on CS could improve the mechanical property of HECS/PVA/BCP hydrogels, and *in vitro* biomineralization treatment could further improve its mechanical performance, as well as its biological capability. First, because of inter- and intramolecular hydrogen bonding and reduction of hydrophilic groups, a 3D interconnected porous structure formed in the CS/PVA matrix.[53] After incorporating BCP NPs into the CS/PVA matrix, the −OH groups on the surface of NPs interact with PVA and CS macromolecules forming interfacial layers. Incorporation of BCP NPs increases the number of hydrophilic moieties, leading to an increase in the interaction of the hydrogel with water molecules via hydrogen bonding.[50] Hydrogen bonding interactions between CS, PVA, and BCP NPs contribute to improving the interface strength of the composites. However, the poor solubility of CS in PVA solvents limits the uniform dispersion of BCP NPs.

HECS, as a derivative of CS with hydroxyethyl groups linked to C-6, shows water solubility and gelling property.[54] It has the potential to directly promote cell migration, growth, and organization during tissue regeneration; therefore, it presents excellent solubility, biocompatibility,[55] and antibacterial properties.[56] HECS molecules uniformly distributed into PVA solution; this could be due to the availability of negatively charged hydroxy groups on HECS that acted as nucleation sites to initiate crystal deposition. The hydroxyethyl group has a better ability to form hydrogen bonds with the hydroxy groups.[57] Compared with pure CS, HECS changes its spatial structure because of the access of the hydroxyethyl group.[54] Several hydrophilic groups on HECS molecules were exposed to interact with PVA and BCP (Scheme 2). Thus, the number of hydrogen bonds formed with HECS, PVA, and BCP NPs increased. Hydrogen bonds promote crystallites during the freezing process,[58] as well as lead to increased rigidity and enhanced mechanical properties.[59] Therefore, compared to the CS/PVA/BCP hydrogel, the more compact and robust pore

https://dx.doi.org/10.1021/acsomega.0c00727
ACS Omega 2020, 5, 10948−10957

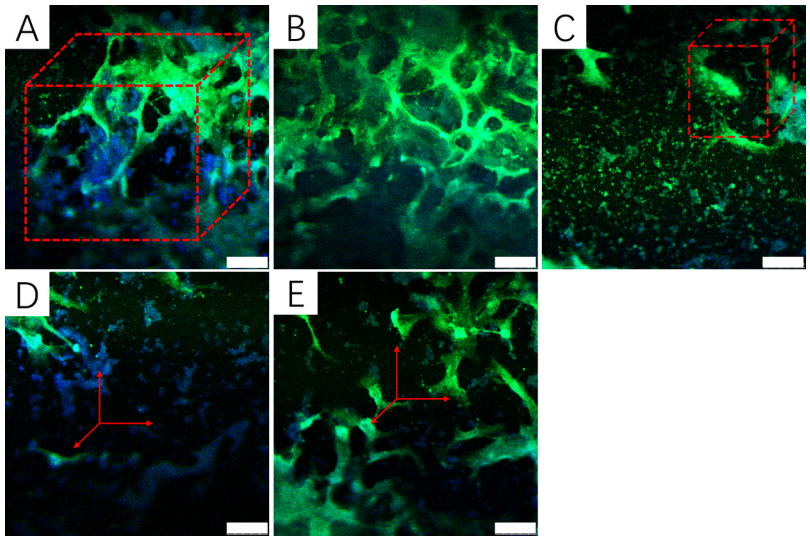

Figure 9. Fluorescence images (phalloidin-FITC/DAPI staining) of hBMSCs after incubation with the prepared HECS/PVA/BCP scaffolds after *in vitro* biomineralization for 5 days: (A): $_{B}$H1; (B): $_{B}$H2; (C) $_{B}$H3; (D) $_{B}$H4; and (E) $_{B}$H5; the scale bar is 50 μm.

Scheme 2. Schematic Diagram of the Mechanism of the Reinforced HECS/PVA/BCP Hydrogels

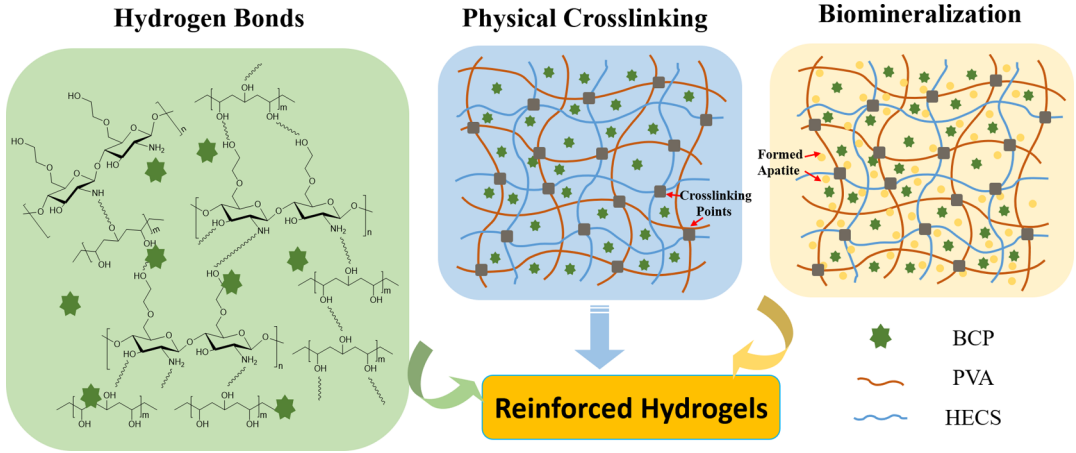

walls in the HECS/PVA/BCP hydrogel increase hydrogen bonds and further lead to the thicker pore wall without nanoscale micropores (Figure 3).

The success of the porous network hydrogel does not only depend on the quality of polymers but also the fabrication methodology. Freeze−thaw method treatment makes PVA produce crystalline microdomains and promotes the physical cross-linking of PVA chains. It could remove the water molecules from the sample to obtain the highly porous architecture hydrogel and provide various sizes of interconnected pores. This process improves the physical cross-linking density of hydrogels and is considered efficient for fabricating the highly porous hydrogel.[60]

Besides, the formation of hydroxyethyl groups on CS chains leads to the increase in the physical cross-linking extent, and the cross-linking points in the HECS/PVA/BCP hydrogel are shown in Scheme 2. The hydrogels exhibited the interconnected porous network structures with regularity and tightness. The decrease in pore size resulted in an increase in cross-linking units. Besides, the compressive strength of the porous hydrogel is manipulated by the microstructure and nature of polymeric materials.[61,62] The appearance of HECS in the PVA solution leads to higher inter- and intramolecular binding forces, provoking the higher strength of the porous structure. These structures significantly improved the rigidity of the network structure and the load-bearing properties. Therefore, the HECS/PVA/BCP hydrogel has higher compressive strength (5−7 MPa) than the CS/PVA/BCP hydrogel (Supporting Information, Figure S7) and CS/PVA/β-TCP hydrogel (2.22 MPa).[50]

On the other hand, *in vitro* biomineralization could further strengthen the HECS/PVA/BCP scaffold. The bone-like apatite depositions were formed and distributed on the pore surface during the *in vitro* biomineralization process (Figure 6). Because of the uniform dispersion of HECS in the PVA solution, the HECS polymer chain provides more sites for the adhesion of calcium and phosphate ions in the surrounding liquid (Scheme 2). Furthermore, the degradation of biomedical implants is another essential factor for BTE, as well as controlling degradation. In our future studies, the *in vitro* and *in vivo* degradation rate of the HECS/PVA/BCP scaffold will be studied.

3. CONCLUSIONS

In summary, the PVA/BCP scaffold was effectively reinforced via using HECS and the *in vitro* biomineralization process.

https://dx.doi.org/10.1021/acsomega.0c00727
ACS Omega 2020, 5, 10948−10957

Because of the hydrogen bonds formed between HECS, PVA, and BCP NPs, the cross-linking efficiency and cross-linking points in HECS/PVA/BCP hydrogels increased, which resulted in the improved compressive strength of the HECS/PVA/BCP hydrogel compared to the CS/PVA/BCP hydrogel without sacrificing the porous structure. Furthermore, the cytocompatibility was further improved via the addition of HECS and in vitro biomineralization. This study suggested that the reinforced HECS/PVA/BCP hydrogel with promising mechanical and biological properties has the potential for application in bone regeneration.

4. EXPERIMENTAL SECTION

4.1. Materials. CS (medium molecular weight, SKU: 448877) with 75−85% deacetylation degree and 200−800 cP viscosity was purchased from Sigma-Aldrich Chemical Reagent Co., Ltd. PVA (polymerization degree ≈ 1799 and hydrolysis degree ≈ 99%), ammonia ($NH_3{\cdot}H_2O$), and calcium nitrate tetrahydrate ($Ca(NO_3)_2{\cdot}4H_2O$) were purchased from Sino-Pharm Chemical Reagent Co., Ltd. Sodium hydroxide (NaOH), hydrochloric acid, isopropanol, anhydrous ethanol, 2-chloroethanol, and ammonium phosphate dibasic ($(NH_4)_2HPO_4$) were purchased from Macklin Biochemical Co., Ltd. All the chemicals were used without further purification.

4.2. Synthesis of HECS. The synthesis of HECS was based on a previous paper with modification on reaction time.[61] About 10 g of CS and 60 g of aqueous 50 wt % NaOH solution were mixed in a three-neck flask and stirred for at least 3 h at room temperature. The mixture was kept at −20 °C for 24 h in a refrigerator. Then, 133 mL of isopropanol was added and refluxed for 90 min in an oil bath, followed by the addition of 18.3 mL of 2-chloroethanol and 33.3 mL of isopropanol. The solution was neutralized using hydrochloric acid, and the resultant solid was purified three times with anhydrous ethanol. Then, the obtained powder was dried in a vacuum oven. Finally, the powder was dialyzed in deionized water for 5 days, and then, the sample was freeze-dried at −60 °C for 72 h to obtain HECS. FTIR spectroscopy (Thermo Fisher, Nicolelis 5) and proton nuclear magnetic resonance (^{1}H NMR 600 MHz NMR spectrometer, JEOL ECZ600R/S3) were used to confirm the successful synthesis of HECS.

4.3. Synthesis of BCP NPs. BCP NPs were prepared by the aqueous precipitation reaction according to our previous studies with further modification.[28,31] $Ca(NO_3)_2{\cdot}4H_2O$ and $(NH_4)_2HPO_4$ solutions with a Ca/P mole ratio of 1.55 were mixed, and the pH of the mixed solution was adjusted to 11 using ammonia at room temperature and stirred for 4 h. The white color precipitate was obtained through centrifugation (3000 rpm), and then, the Millipore water was added; this process was repeated many times until the pH of the solution was neutral. The precipitate was kept in an oven at 80 °C to acquire the white powder after drying. Finally, the sample was placed in a muffle furnace and treated at 1125 °C for 1 h, and BCP NPs were obtained using a ball grinding machine (FOCUCY, F-P2000).

4.4. Fabrication of the Porous HECS/PVA/BCP Scaffold. Initially, HECS was dissolved in a 2 wt % acetic acid solution to prepare the HECS solution, and the PVA powder was dissolved in deionized water and stirred at 90 °C for 3 h to obtain an 8 wt % PVA solution. The HECS solution and PVA solution were mixed and stirred for 30 min, and the BCP NP powder was added into the mixed solution and stirred for 24 h. The mixed solution was poured into a 24-well plate and kept in a vacuum oven for 2 h to degas the samples, and then, the samples were frozen at −20 °C for 12 h and thawed subsequently at room temperature for 1 h. After three freeze−thaw cycles, the samples were washed with Millipore water to remove acetic acid and lyophilized at −65 °C for 72 h to obtain the porous HECS/PVA/BCP scaffold. In this paper, we fabricated five different samples with different HECS/PVA/BCP weight ratios, as shown in Table 1 and Figure S1 (Supporting Information). Also, the CS/PVA/BCP scaffolds with the same method were prepared for comparison, as shown in Table S1.

Table 1. Composition and Content of the HECS/PVA/BCP Nanocomposite Hydrogels

sample	H1	H2	H3	H4	H5
HECS (%)	18.18	15.38	13.33	9.52	8.70
PVA[a] (%)	54.55	61.54	66.67	76.19	78.26
BCP (%)	27.27	23.08	20.00	14.29	13.04

[a]8 wt % PVA solution was used to prepare all samples.

4.5. In Vitro Biomineralization of HECS/PVA/BCP Scaffolds. The prepared HECS/PVA/BCP scaffolds were *in vitro* biomineralized using a cell culture medium (Scheme 1). Briefly, the lyophilized samples were placed into a 6-well cell plate and covered with DMEM containing FBS (10 wt %) in a sterile environment. The plates were kept in an incubator at 37 °C, and the medium was changed every 2 days. After 5 days, the samples were taken out and lyophilized for 72 h. $_B$H represented the HECS/PVA/BCP scaffold after *in vitro* biomineralization treatment.

4.6. Characterization. *4.6.1. Morphology.* The morphology of BCP NPs was observed using a transmission electron microscope (FEI Tecnai G2 F20). The BCP NPs were dispersed in ethanol, treated for 30 min using ultrasonic equipment, and deposited on the copper grid. The microstructure of porous HECS/PVA/BCP and CS/PVA/BCP scaffolds was observed using a cold-field scanning electron microscope (Hitachi, S-4800). Before observation, the samples were coated with platinum.

4.6.2. Fourier Transform Infrared Spectroscopy. FTIR spectroscopy (Thermo Fisher, Nicolelis 5) was used to test the presence of specific chemical groups in raw materials and different scaffolds. FTIR spectra were obtained within the range between 4000 and 500 cm^{-1} on the FTIR spectrometer with a resolution of 1 cm^{-1} and using the attenuated total reflectance technique for testing solid scaffold samples.

4.6.3. X-ray Diffraction. BCP NPs were analyzed using the XRD (Rigaku Smartlab 9 kW diffractometer) test. The data were recorded over a range of $10° \leq 2\theta \leq 90°$, with continuous scans at a rate of 0.02° min^{-1}, using a copper ray tube operated at 45 kV and 15 mA.

4.6.4. Porosity. The porosity (P) of scaffolds was measured using a liquid displacement method.[5,28,31] First, the dried scaffold was submerged in a known volume (V_1) of ethanol. The volume of the sample-impregnated liquid was measured and recorded as V_2. When removing the liquid-impregnated scaffold, the remaining liquid volume was measured and recorded as V_3. Then, the porosity could be calculated using the following formula

$$P = (V_1 - V_3)/(V_2 - V_3) \times 100\%$$

https://dx.doi.org/10.1021/acsomega.0c00727
ACS Omega 2020, 5, 10948−10957

4.6.5. Mechanical Properties. The uniaxial compression test was performed to measure the mechanical behavior of the prepared scaffolds. The different testing method was used here compared to our previous papers.[27,28,31] All the measurements were completed at room temperature using a microcomputer control electronic universal testing machine (CMT-4103, Zhuhai, China). The crosshead speed was set at 4 mm/min, and the load cell was set at 0.9 kN. The compressive strength (C_s) of the scaffold was calculated using the below equation

$$C_s = F/m$$

where F is the load at the time of the fracture and m represents the cross-sectional area of the samples.

4.6.6. Swelling Behavior. The swelling capacity of the scaffold was studied by incubating the sample in PBS at 37 °C. All samples were weighed before the test. In a specified time interval (20 min), the sample was taken out, placed on a filter paper to remove the liquid on the surface, and weighed. The following formula determines the water absorption rate

$$\text{water absorption rate} = (W_t - W_0)/W_0 \times 100\%$$

W_0 represents the weight of the initial sample and W_t represents the weight measured at the predetermined time point.

4.6.7. In Vitro hBMSC Culture. hBMSCs (Normal, Human, ATCCPCS-500-012) were used for toxicity testing here. According to ATCC instructions, the cells were cultured at 37 °C in the environment of 5% CO_2. Cells were seeded in DMEM with 10% FBS and 1% of a 100 mg/mL mixture of streptomycin and penicillin. The cells at passage 5 were used for the following experiments.

4.6.8. hBMSC Growth in the Scaffold. The obtained scaffolds were cut into smaller cubes, soaked in 75% ethanol for 12 h, and irradiated with UV for 6 h. Then, the samples were washed many times using PBS to replace the ethanol inside. The samples were put into the 24-well plate and treated by UV irradiation for 30 min. After that, 1×10^5 cell solution was added (1 mL of cell solution was diluted into 24 mL and 1 mL for each well; the cell solution was directly dropped on the surface of the scaffold). The cells/scaffold was cultured under a humidified atmosphere of 95% air and 5% CO_2 at 37 °C. The cell medium was changed every 24 h; the growth of cells in scaffolds and morphology of cells were investigated using CCK-8 analysis and fluorescent staining, respectively.

4.6.9. CCK-8. hBMSC viability in the scaffold was quantitatively investigated using Cell Counting Kit-8 (CCK-8). At days 1, 2, and 3, 100 μL of CCK-8 solution was added to the sample, and cultured at 37 °C in a CO_2 incubator for 4 h to form formazan crystals. Then, the liquid was transferred to a 96-well plate. The absorbance of each well was measured at 570 nm using an enzyme-linked immunosorbent assay plate reader (Bio-Rad). In this study, cells without scaffolds were used as a control group.

4.6.10. Fluorescent Microscopy Observation. After the scaffolds were cultured with hBMSCs for 3 days, glutaraldehyde was used to fix the seeded cells inside the scaffolds. The scaffolds were removed from the cell medium and washed three times with PBS; then, the cell membrane was permeabilized with 0.1% TRITON X-100 at 37 °C for 10 min and washed with PBS again. Next, 1 mL of 1% BSA was added and kept for 30 min, and 100 μL of 5 μg/mL phalloidin-FITC (Invitrogen, USA) was added under a dark environment for 1 h. The sample was washed three times with PBS, and 200 μL of 1% DAPI solution was added to protect it from light for 10 min. Finally, 400 μL of DAPI (Thermo Scientific) was added in the dark for 5 min. Finally, the samples were washed three times with PBS and observed under a confocal laser scanning microscope (CLSM, Leica TCS SP5 II, Germany).

4.7. Statistical Analysis. Each experiment was performed in triplicate if without a particular explanation, and the results are expressed as means ± SDs. Statistical analyses were performed using the SPSS software package. Levene's test was performed to determine the homogeneity of variance for all the data, and then, Tamhane Post Hoc tests were performed for the comparison between different groups. Different p values of <0.05 (*), <0.01 (**), and <0.001 (***) were considered as statistically significant.

■ ASSOCIATED CONTENT

Supporting Information

The Supporting Information is available free of charge at https://pubs.acs.org/doi/10.1021/acsomega.0c00727.

Macroscopic images of HECS/PVA/BCP hydrogels with different HECS ratio; ^{1}H NMR spectrum of HECS; XRD spectra of the prepared BCP NPs; SEM images of the CS/PVA/BCP hydrogel with different CS/PVA/BCP ratios and the HECS/PVA/BCP hydrogel at lower magnification; pore size distribution of the HECS/PVA/BCP hydrogels; compressive strength of the prepared CS/PVA/BCP hydrogels; and in vitro cytocompatibility of the prepared CS/PVA/BCP scaffolds and HECS/PVA/BCP scaffolds without *in vitro* biomineralization treatment via culturing with hBMSCs for different days (PDF)

■ AUTHOR INFORMATION

Corresponding Authors

Lei Nie − *College of Life Sciences, Xinyang Normal University, Xinyang 464000, China; Department of Mechanical Engineering, Member of Flanders Make, KU Leuven (Catholic University of Leuven), Leuven 3001, Belgium;* orcid.org/0000-0002-6175-5883; Phone: +86-13600621068; Email: nieleifu@yahoo.com, nielei@xynu.edu.cn

Amin Shavandi − *BioMatter Unit—École Polytechnique de Bruxelles, Université Libre de Bruxelles, Brussels 1050, Belgium;* Email: amin.shavandi@ulb.be

Authors

Yaling Deng − *College of Mechanical and Electronic Engineering, Nanjing Forestry University, Nanjing 210037, P. R. China;* orcid.org/0000-0003-0328-0450

Pei Li − *College of Life Sciences, Xinyang Normal University, Xinyang 464000, China; Key Laboratory of Molecular Biophysics of the Ministry of Education, College of Life Science & Technology, Huazhong University of Science and Technology, Wuhan 430074, China*

Ruixia Hou − *Medical School of Ningbo University, Ningbo 315211, P. R. China*

Shoufeng Yang − *Department of Mechanical Engineering, Member of Flanders Make, KU Leuven (Catholic University of Leuven), Leuven 3001, Belgium*

Complete contact information is available at: https://pubs.acs.org/10.1021/acsomega.0c00727

https://dx.doi.org/10.1021/acsomega.0c00727
ACS Omega 2020, 5, 10948−10957

Author Contributions

[¶]L.N. and Y.D. contributed equally to this work and should be considered co-first authors.

Notes

The authors declare no competing financial interest.

■ ACKNOWLEDGMENTS

This research was funded by the National Natural Science Foundation of China (31700840) and the China Postdoctoral Science Foundation (2018M632310). This research was supported by the Nanhu Scholars Program for Young Scholars of XYNU. The authors would like to acknowledge the Analysis & Testing Center of XYNU for the use of their equipment.

■ REFERENCES

(1) Petite, H.; Viateau, V.; Bensaïd, W.; Meunier, A.; de Pollak, C.; Bourguignon, M.; Oudina, K.; Sedel, L.; Guillemin, G. Tissue-Engineered Bone Regeneration. *Nat. Biotechnol.* **2000**, *18*, 959−963.
(2) Shrivats, A. R.; McDermott, M. C.; Hollinger, J. O. Bone Tissue Engineering: State of the Union. *Drug Discovery Today* **2014**, *19*, 781−786.
(3) García-Gareta, E.; Coathup, M. J.; Blunn, G. W. Osteoinduction of Bone Grafting Materials for Bone Repair and Regeneration. *Bone* **2015**, *81*, 112−121.
(4) Fibbe, W. E.; Dazzi, F.; LeBlanc, K. MSCs: Science and Trials. *Nat. Med.* **2013**, *19*, 812−813.
(5) Shavandi, A.; Bekhit, A. E.-D. A.; Ali, M. A.; Sun, Z. F. Bio-mimetic Composite Scaffold from Mussel Shells, Squid Pen and Crab Chitosan for Bone Tissue Engineering. *Int. J. Biol. Macromol.* **2015**, *80*, 445−454.
(6) Wu, S.; Liu, X.; Yeung, K. W. K.; Liu, C.; Yang, X. Biomimetic Porous Scaffolds for Bone Tissue Engineering. *Mater. Sci. Eng., R* **2014**, *80*, 1−36.
(7) Cheng, A.; Schwartz, Z.; Kahn, A.; Li, X.; Shao, Z.; Sun, M.; Ao, Y.; Boyan, B. D.; Chen, H. Advances in Porous Scaffold Design for Bone and Cartilage Tissue Engineering and Regeneration. *Tissue Eng., Part B* **2019**, *25*, 14−29.
(8) Levengood, S. K. L.; Zhang, M. Chitosan-Based Scaffolds for Bone Tissue Engineering. *J. Mater. Chem. B* **2014**, *2*, 3161−3184.
(9) Roy, P.; Sailaja, R. R. N. Chitosan-nanohydroxyapatite Composites: Mechanical, Thermal and Bio-compatibility Studies. *Int. J. Biol. Macromol.* **2015**, *73*, 170−181.
(10) Bandyopadhyay, A.; Bernard, S.; Xue, W.; Bose, S. Calcium Phosphate-based Resorbable Ceramics: Influence of MgO, ZnO, and SiO_2 Dopants. *J. Am. Ceram. Soc.* **2006**, *89*, 2675−2688.
(11) Bonjour, J.-P. Calcium and Phosphate: A Duet of Ions Playing for Bone Health. *J. Am. Coll. Nutr.* **2011**, *30*, 438S−448S.
(12) Bohner, M. Resorbable Biomaterials as Bone Graft Substitutes. *Mater. Today* **2010**, *13*, 24−30.
(13) Bohner, M.; Galea, L.; Doebelin, N. Calcium Phosphate Bone Graft Substitutes: Failures and Hopes. *J. Eur. Ceram. Soc.* **2012**, *32*, 2663−2671.
(14) Val, J. E. M.; Mazón, P.; Guirado, J. L. C.; Ruiz, R. A. D.; Fernández, M. P. R.; Negri, B.; Abboud, M.; Aza, P. N. D. Comparison of Three Hydroxyapatite/b-Tricalcium Phosphate/Collagen Ceramic Scaffolds: An in Vivo Study. *J. Biomed. Mater. Res., Part A* **2013**, *102*, 1037−1046.
(15) Garrido, C. A.; Lobo, S. E.; Turíbio, F. M.; Legeros, R. Z. Biphasic Calcium Phosphate Bioceramic for Orthopaedic Reconstructions: Clinical Outcomes. *Int. J. Biomater.* **2011**, *2011*, 1−9.
(16) Huang, Y.; Zhou, G.; Zheng, L.; Liu, H.; Niu, X.; Fan, Y. Micro-/Nano-sized Hydroxyapatite Directs Differentiation of Rat Bone Marrow Derived Mesenchymal Stem Cells Towards an Osteoblast Lineage. *Nanoscale* **2012**, *4*, 2484−2490.
(17) He, F.; Qian, G.; Ren, W.; Li, J.; Fan, P.; Shi, H.; Shi, X.; Deng, X.; Wu, S.; Ye, J. Fabrication of β-Tricalcium Phosphate Composite Ceramic Sphere-Based Scaffolds with Hierarchical Pore Structure for Bone Regeneration. *Biofabrication* **2017**, *9*, 025005.
(18) Marchi, J.; Ribeiro, C.; Bressiani, A. H. d. A.; Marques, M. M. Cell Response of Calcium Phosphate Based Ceramics, A Bone Substitute Material. *Mater. Res.* **2013**, *16*, 703−712.
(19) Victoria, E. C.; Gnanam, F. D. Synthesis and Characterisation of Biphasic Calcium Phosphate. *Trends Biomater. Artif. Organs* **2002**, *16*, 12−14.
(20) Yang, Y.; He, F.; Ye, J. Preparation, Mechanical Property and Cytocompatibility of Freeze-Cast Porous Calcium Phosphate Ceramics Reinforced by Phosphate-Based Glass. *Mater. Sci. Eng., C* **2016**, *69*, 1004−1009.
(21) Mestres, G.; Le Van, C.; Ginebra, M.-P. Silicon-Stabilized α-Tricalcium Phosphate and Its Use in A Calcium Phosphate Cement: Characterization and Cell Response. *Acta Biomater.* **2012**, *8*, 1169−1179.
(22) Roohani-Esfahani, S. I.; Lu, Z. F.; Li, J. J.; Ellis-Behnke, R.; Kaplan, D. L.; Zreiqat, H. Effect of Self-Assembled Nanofibrous Silk/Polycaprolactone Layer on The Osteoconductivity and Mechanical Properties of Biphasic Calcium Phosphate Scaffolds. *Acta Biomater.* **2012**, *8*, 302−312.
(23) Bouler, J. M.; Pilet, P.; Gauthier, O.; Verron, E. Biphasic Calcium Phosphate Ceramics for Bone Reconstruction: A Review of Biological Response. *Acta Biomater.* **2017**, *53*, 1−12.
(24) Kim, H.-W.; Knowles, J. C.; Kim, H.-E. Hydroxyapatite/Poly(ε-caprolactone) Composite Coatings on Hydroxyapatite Porous Bone Scaffold for Drug Delivery. *Biomaterials* **2004**, *25*, 1279−1287.
(25) Nguyen, T. B. L.; Lee, B.-T. A Combination of Biphasic Calcium Phosphate Scaffold with Hyaluronic Acid-Gelatin Hydrogel as a New Tool for Bone Regeneration. *Tissue Eng., Part A* **2014**, *20*, 1993−2004.
(26) Lan, W.; Zhang, X.; Xu, M.; Zhao, L.; Huang, D.; Wei, X.; Chen, W. Carbon Nanotube Reinforced Polyvinyl Alcohol/Biphasic Calcium Phosphate Scaffold for Bone Tissue Engineering. *RSC Adv.* **2019**, *9*, 38998−39010.
(27) Nie, L.; Wu, Q.; Long, H.; Hu, K.; Li, P.; Wang, C.; Sun, M.; Dong, J.; Wei, X.; Suo, J.; Hua, D.; Liu, S.; Yuan, H.; Yang, S. Development of Chitosan/Gelatin Hydrogels Incorporation of Biphasic Calcium Phosphate Nanoparticles for Bone Tissue Engineering. *J. Biomater. Sci., Polym. Ed.* **2019**, *30*, 1636−1657.
(28) Nie, L.; Chen, D.; Fu, J.; Yang, S.; Hou, R.; Suo, J. Macroporous Biphasic Calcium Phosphate Scaffolds Reinforced by Poly-L-lactic acid/Hydroxyapatite Nanocomposite Coatings for Bone Regeneration. *Biochem. Eng. J.* **2015**, *98*, 29−37.
(29) Padalhin, A. R.; Thuy Ba Linh, N.; Ki Min, Y.; Lee, B.-T. Evaluation of The Cytocompatibility Hemocompatibility in Vivo Bone Tissue Regenerating Capability of Different PCL Blends. *J. Biomater. Sci., Polym. Ed.* **2014**, *25*, 487−503.
(30) Kumar, A.; Negi, Y. S.; Choudhary, V.; Bhardwaj, N. K. Effect of modified cellulose nanocrystals on microstructural and mechanical properties of polyvinyl alcohol/ovalbumin biocomposite scaffolds. *Mater. Lett.* **2014**, *129*, 61−64.
(31) Nie, L.; Chen, D.; Suo, J.; Zou, P.; Feng, S.; Yang, Q.; Yang, S.; Ye, S. Physicochemical Characterization and Biocompatibility in Vitro of Biphasic Calcium Phosphate/Polyvinyl Alcohol Scaffolds Prepared by Freeze-Drying Method for Bone Tissue Engineering Applications. *Colloids Surf., B* **2012**, *100*, 169−176.
(32) Chen, G.; Chen, N.; Wang, Q. Fabrication and Properties of Poly(vinyl alcohol)/β-Tricalcium Phosphate Composite Scaffolds via Fused Deposition Modeling for Bone Tissue Engineering. *Compos. Sci. Technol.* **2019**, *172*, 17−28.
(33) Părpăriţăa, E.; Cheaburua, C. N.; Paţachia, S. F.; Vasilea, C. Polyvinyl alcohol/chitosan/montmorillonite nanocomposites preparation by freeze/thaw cycles and characterization. *Acta Chem. Iasi* **2014**, *22*, 75−96.
(34) Zolghadri, M.; Samandari, S.; Ahmadi, S.; Alamara, K. Synthesis and characterization of porous cytocompatible scaffolds from polyvinyl-chitosan. *Bull. Mater. Sci.* **2019**, *42*, 35.

https://dx.doi.org/10.1021/acsomega.0c00727
ACS Omega 2020, 5, 10948−10957

(35) Seol, Y.-J.; Lee, J.-Y.; Park, Y.-J.; Lee, Y.-M.; Ku, Y.; Rhyu, I.-C.; Lee, S.-J.; Han, S.-B.; Chung, C.-P. Chitosan Sponges As Tissue Engineering Scaffolds for Bone Formation. *Biotechnol. Lett.* **2004**, *26*, 1037−1041.
(36) Shavandi, A.; Bekhit, A. E.-D. A.; Sun, Z.; Ali, M. A. Injectable Gel From Squid Pen Chitosan for Bone Tissue Engineering Applications. *J. Sol-Gel Sci. Technol.* **2016**, *77*, 675−687.
(37) Shavandi, A.; Bekhit, A. A.; Bekhit, A. E.-D. A.; Sun, Z.; Ali, M. A. Preparation and Characterisation of Irradiated Crab Chitosan and New Zealand Arrow Squid Pen Chitosan. *Mater. Chem. Phys.* **2015**, *167*, 295−302.
(38) Jamalpoor, Z.; Mirzadeh, H.; Joghataei, M. T.; Zeini, D.; Bagheri-Khoulenjani, S.; Nourani, M. R. Fabrication of Cancellous Biomimetic Chitosan-Based Nanocomposite Scaffolds Applying a Combinational Method for Bone Tissue Engineering. *J. Biomed. Mater. Res., Part A* **2015**, *103*, 1882−1892.
(39) Saravanan, S.; Leena, R. S.; Selvamurugan, N. Chitosan based biocomposite scaffolds for bone tissue engineering. *Int. J. Biol. Macromol.* **2016**, *93*, 1354−1365.
(40) Duan, B.; Wu, L.; Li, X.; Yuan, X.; Li, X.; Zhang, Y.; Yao, K. Degradation of Electrospun PLGA-Chitosan/PVA Membranes and Their Cytocompatibility in Vitro. *J. Biomater. Sci., Polym. Ed.* **2007**, *18*, 95−115.
(41) Koyano, T.; Koshizaki, N.; Umehara, H.; Nagura, M.; Minoura, N. Surface States of PVA/Chitosan Blended Hydrogels. *Polymer* **2000**, *41*, 4461−4465.
(42) Sin, L. T.; Rahman, W. A. W. A.; Rahmat, A. R.; Khan, M. I. Detection of Synergistic Interactions of Polyvinyl Alcohol-Cassava Starch Blends Through DSC. *Carbohydr. Polym.* **2010**, *79*, 224−226.
(43) Kanimozhi, K.; Khaleel Basha, S.; Sugantha Kumari, V. Processing and Characterization of Chitosan/PVA and Methylcellulose Porous Scaffolds for Tissue Engineering. *Mater. Sci. Eng., C* **2016**, *61*, 484−491.
(44) Takei, T.; Nakahara, H.; Ijima, H.; Kawakami, K. Synthesis of A Chitosan Derivative Soluble at Neutral pH And Gellable by Freeze-Thawing, and Its Application in Wound Care. *Acta Biomater.* **2012**, *8*, 686−693.
(45) El-Sherbiny, I. M. Synthesis, Characterization and Metal Uptake Capacity of a New Carboxymethyl Chitosan Derivative. *Eur. Polym. J.* **2009**, *45*, 199−210.
(46) Zhao, Y.; Chen, J.; Zeng, E.; Hu, X.; Liu, A.; Dong, Y. Synthesis and Characterization of Hydroxyethyl Chitosan Grafted by Carboxyl Ending DOVOB Dendrimer: A Novel Liquid Crystalline Polymer. *Carbohydr. Polym.* **2008**, *74*, 828−833.
(47) Qiao, X.; Peng, X.; Qiao, J.; Jiang, Z.; Han, B.; Yang, C.; Liu, W. Evaluation of A Photocrosslinkable Hydroxyethyl Chitosan Hydrogel As a Potential Drug Release System for Glaucoma Surgery. *J. Mater. Sci.: Mater. Med.* **2017**, *28*, 149.
(48) Kumar, M. S.; Khan, F. L. A. Quantitative Prediction of Urinary Stone Samples Using Partial Least Square Regression Coupled with FTIR Spectra. *Int. J. Adv. Sci. Tech. Res.* **2016**, *6*, 393−403.
(49) Hollister, S. J. Scaffold Design and Manufacturing: From Concept to Clinic. *Adv. Mater.* **2009**, *21*, 3330−3342.
(50) Ali, A.; Bano, S.; Priyadarshi, R.; Negi, Y. S. Effect of Carbon Based Fillers on Properties of Chitosan/PVA/βTCP Based Composite Scaffold for Bone Tissue Engineering. *Mater. Today: Proc.* **2019**, *15*, 173−182.
(51) Nie, L.; Wang, C.; Hou, R. X.; Li, X. Y.; Sun, M.; Suo, J. P.; Wang, Z.; Cai, R. H.; Yin, B.; Fang, L.; Wei, X. Y.; Yuan, H. Y. Preparation and Characterization of Dithiol-Modified Graphene Oxide Nanosheets Reinforced Alginate Nanocomposite as Bone Scaffold. *SN Appl. Sci.* **2019**, *1*, 545.
(52) Nie, L.; Li, X.; Wang, Z.; Hu, K.; Cai, R.; Li, P.; Han, Y.; Sun, M.; Yuan, H.; Suo, J.; Yang, S. Vitro Biomineralization on Polyvinyl Alcohol/Biphasic Calcium Phosphate Hydrogels. *Bioinspired, Biomimetic Nanobiomater.* **2019**, *0*, 1−7.
(53) Nair, M.; Nancy, D.; Krishnan, A. G.; Anjusree, G. S.; Vadukumpully, S.; Nair, S. V. Graphene Oxide Nanoflakes Incorporated Gelatin-Hydroxyapatite Scaffolds Enhance Osteogenic Differentiation of Human Mesenchymal Stem Cells. *Nanotechnology* **2015**, *26*, 161001.
(54) Shao, K.; Han, B.; Gao, J.; Song, F.; Yang, Y.; Liu, W. Synthesis and Characterization of A Hydroxyethyl Derivative of Chitosan and Evaluation of Its Biosafety. *J. Ocean Univ. China* **2015**, *14*, 703−709.
(55) Liang, Y.; Liu, W.; Han, B.; Yang, C.; Ma, Q.; Zhao, W.; Rong, M.; Li, H. Fabrication and Characters of A Corneal Endothelial Cells Scaffold Based on Chitosan. *J. Mater. Sci.: Mater. Med.* **2011**, *22*, 175−183.
(56) Liu, H.; Zhao, Y.; Cheng, S.; Huang, N.; Leng, Y. Syntheses of Novel Chitosan Derivative with Excellent Solubility, Anticoagulation, and Antibacterial Property by Chemical Modification. *J. Appl. Polym. Sci.* **2011**, *124*, 2641−2648.
(57) Luo, K.; Yin, J.; Khutoryanskaya, O. V.; Khutoryanskiy, V. V. Mucoadhesive and Elastic Films Based on Blends of Chitosan and Hydroxyethylcellulose. *Macromol. Biosci.* **2008**, *8*, 184−192.
(58) Ou, K.; Dong, X.; Qin, C.; Ji, X.; He, J. Properties and Toughening Mechanisms of PVA/PAM Double-Network Hydrogels Prepared by Freeze-Thawing and Anneal-Swelling. *Mater. Sci. Eng., C* **2017**, *77*, 1017−1026.
(59) Hu, D.; Wang, H.; Wang, L. Physical Properties and Antibacterial Activity of Quaternized Chitosan/Carboxymethyl Cellulose Blend Films. *LWT–Food Sci. Technol.* **2016**, *65*, 398−405.
(60) Croisier, F.; Jérôme, C. Chitosan-Based Biomaterials for Tissue Engineering. *Eur. Polym. J.* **2013**, *49*, 780−792.
(61) Wang, Y.; Qian, J.; Zhao, N.; Liu, T.; Xu, W.; Suo, A. Novel Hydroxyethyl Chitosan/Cellulose Scaffolds with Bubble-like Porous Structure for Bone Tissue Engineering. *Carbohydr. Polym.* **2017**, *167*, 44−51.
(62) Stammen, J. A.; Williams, S.; Ku, D. N.; Guldberg, R. E. Mechanical Properties of a Novel PVA Hydrogel in Shear And Unconfined Compression. *Biomaterials* **2001**, *22*, 799−806.

https://dx.doi.org/10.1021/acsomega.0c00727
ACS Omega 2020, 5, 10948−10957